Microchimica Acta (2018) 185: 320
https://doi.org/10.1007/s00604-018-2838-y

ORIGINAL PAPER

Voltammetric aptasensor for bisphenol A based on the use of a MWCNT/Fe_3O_4@gold nanocomposite

Mehdi Baghayeri[1] · Reza Ansari[2] · Marzieh Nodehi[2] · Iman Razavipanah[3] · Hojat Veisi[4]

Received: 26 April 2018 / Accepted: 6 May 2018 / Published online: 7 June 2018

Abstract

The present study describes an electrochemical aptamer-based method for the determination of bisphenol A (BPA). It is making use of gold nanoparticles (AuNPs) immobilized on a conjugate between multiwalled carbon nanotubes and thiol-functionalized magnetic nanoparticles (MWCNT/Fe_3O_4-SH) that are modified with an aptamer. The nanocomposite was characterized by Fourier transform infrared spectroscopy, field emission scanning electron microscopy, transmission electron microscopy, vibrating sample magnetometry, elemental mapping analysis and energy dispersive X-ray diffraction. The aptasensor, typically operated at 0.20 V (vs. Ag/AgCl), has a linear response in the 0.1 to 8 nM BPA concentration range, a low detection limit (0.03 nM), and high sensitivity (86.43 μA nM^{-1} cm^{-2}). Voltammetric experiments were performed by using the hexacyanoferrate redox system as an electrochemical probe. The results indicate that the presence of AuNPs, magnetic nanoparticles and MWCNTs results a synergistic electrochemical augmentation. The method is highly selective, sensitive, efficient and environmentally friendly. The method was successfully applied to the determination of BPA in spiked real samples.

Keywords Electrochemical biosensor · Hexacyanoferrate · Aptamer · Gold nanoparticles · Multiwalled carbon nanotubes · Magnetic nanoparticles

Introduction

Bisphenol A (BPA) is a harmful endocrine disrupting chemical that is extensively used in the industrial production of polycarbonate plastics and epoxy resins, which are important components in the production of beverage bottles, baby bottles, children's toys, and also the inner surface coating of cans used for food and the like [1]. Plastics Europe (PEMRG) reported that the production volume of plastics exceeds 299 million tons in the world, and that more than 9.6 million tons of plastics waste are land-filled every year in Europe [2]. However, the European Food Safety Authority (EFSA) reported that the Daily Intake (TDI) level for BPA currently tolerable is 4 μg kg^{-1} body weight per day [1]. Fortunately, many effective measures have been taken to control the adverse effects of BPA. For example, the use of BPA in the production of baby bottles has been banded in many countries [3], Moreover, in Europe, the production level of plastics has remained constant since 2013 after the 2009 turndown, with the actual levels being similar to those in 2002 [2]. Because of the negative effects of BPA on the environment and human health, the detection of BPA is urgently needed both for food safety concerns, and environmental monitoring. So far, the typical analytical methods for the detection and determination of BPA have been solid phase microextraction-spectrophotometry [4], liquid chromatography (LC) [5], liquid chromatographic-mass spectrometry (LC-MS) [6], gas chromatography-mass spectrometry (GC-MS) and capillary electrophoresis [7, 8]. However, the majority of these techniques suffer a number of serious limitations including the need for skilled personnel, time-consuming pretreatment processes and high cost of the

Electronic supplementary material The online version of this article (https://doi.org/10.1007/s00604-018-2838-y) contains supplementary material, which is available to authorized users.

✉ Mehdi Baghayeri
m.baghayeri@hsu.ac.ir

[1] Department of Chemistry, Faculty of Science, Hakim Sabzevari University, PO. Box 397, Sabzevar, Iran

[2] Department of Chemistry, Faculty of Science, University of Guilan, Namjoo Street, PO. Box 1914, Rasht, Iran

[3] Department of Chemistry, Faculty of Sciences, Ferdowsi University of Mashhad, Mashhad, Iran

[4] Department of Chemistry, Payame Noor University, Tehran 19395-4697, Iran

instruments [9]. The electrochemical sensors have made the BPA detection simpler, faster, and more economic [10]. However, these electrochemical sensors have a moderate selectivity index.

Aptamers are short single-stranded ssDNA or RNA oligonucleotides which can serve a function similar to that of antibodies, when synthesized in vitro evolution process with high reproducibility and purity [11]. The use of aptamers as recognizing receptors in different biosensor designs especially, in electrochemical biosensors, is very promising and attractive due to their advantages: their suitability for the detection of small molecule analytes, low cost of production, high flexibility, high selectivity due to strong affinity between anti-aptamers and their target, and the relative ease of modification by adding functional groups [12]. Therefore, from among all BPA sensors, electrochemical aptasensors has been considered preferable for the detection of BPA. For example, Zhu et al. reported high sensitivity and selectivity indices and a detection limit of 0.056 nM for a biosensor based on aptamer-functionalized nanoporous gold film (NPGF) used for the direct electrochemical detection of BPA [13]. In another study, Liu et al. reported a signal-off aptasensor based on a gold-modified glassy carbon electrode [14]. Derikvand et al. deposited a glassy carbon electrode surface with highly dispersed platinum nanoparticles on acid-oxidized carbon nanotubes and functionalized with polyethyleneimine [15]. Cui et al. reported a label-free and single-step method for detection of bisphenol A. They used aptamar as a probe molecule and commercially available array of interdigitated aluminum microelectrodes as an immobilization ptatform for determination of BPA in aqueous solution [16].

The use of magnetic nanoparticles (MNPs) in the development of sensing devices has received significant attention due to their properties including chemical inertness, magnetic properties, non-toxicity, and thermal stability. More recently, the present research team reported the fabrication of electrochemical biosensors based on iron oxide magnetic nanoparticles, functionalized with different polymers and copolymers [17–19]. If an efficient chemical compound with special functional groups is selected and immobilized on MNPs, it will be possible to modify them with other heterogeneous nanomaterials, and increase their operational performance in a variety of applications. Moreover, in such structures, if noble metals with nanosized crystals are used, they can act as a key signal receiver, thus enhancing the electrochemical signal of an analyt [20]. Tian et al. synthesized

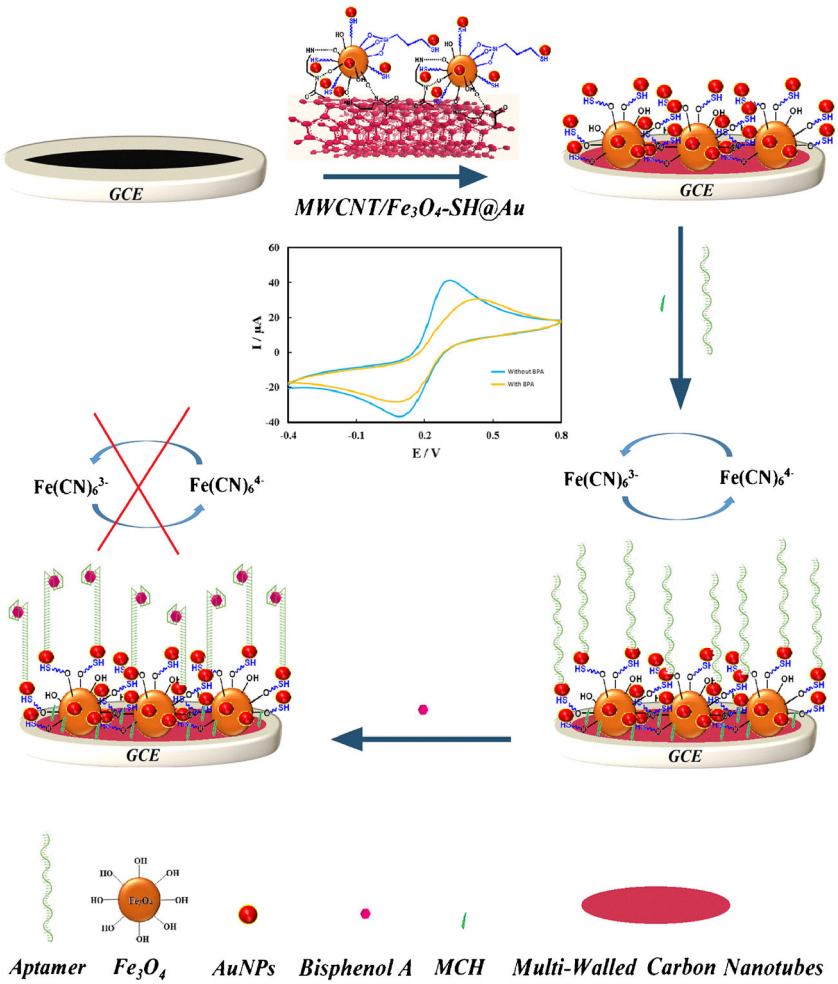

Scheme 1 Preparation of GCE/MWCNT/Fe_3O_4-SH@Au/aptamer/MCH electrode

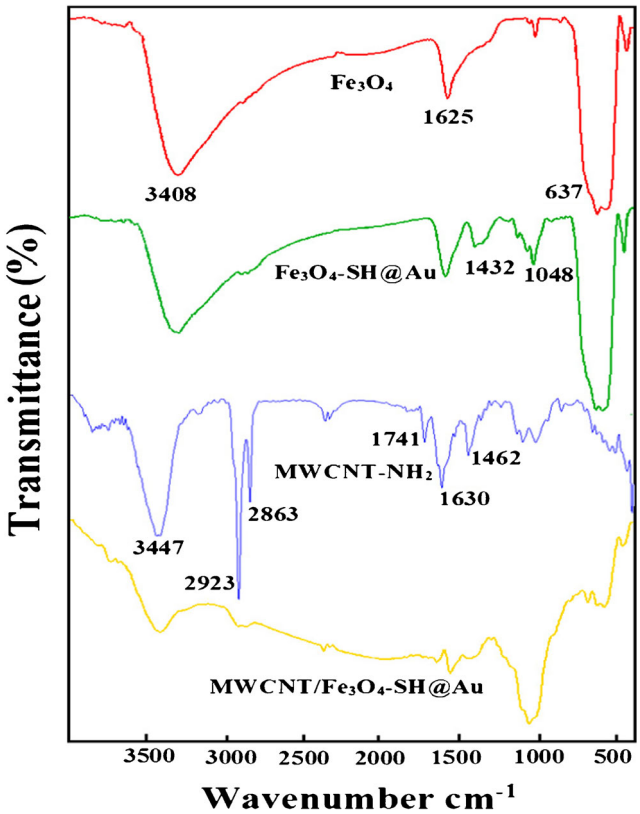

Fig. 1 The FT-IR spectra of Fe_3O_4, Fe_3O_4-SH@Au, MWCNTs-NH_2 and MWCNT/Fe_3O_4-SH@Au nanocomposite

nanocomposite based on Au-nanorod and Fe_3O_4NPs by the decomposition of Fe(acac)$_3$ onto Au-nanorods for determination of 4-aminothiophenol [21]. Additionally, large surface areas of noble metals provide occasion for the stable immobilization of biomolecules and their conductivity simplify the electron transfer between biological molecules and electrode surface for the construction of electrochemical biosensors. Zhou et al. proposed the use of electrochemical aptasensor based on gold nanoparticles dotted graphene (GNPs/GR) nanocomposite film modified glassy carbon for the determination of BPA in milk products [22]. MWCNT-modified electrodes have been useful to accumulate important biomolecules and to reduce surface fouling effects. Deiminiat et al. developed gold electrode modified by a functionalized multiwall carbon nanotubes/gold nanoparticles (f-MWCNTs/AuNPs) nanocomposite film to be used for the examination of BPA in real sample with a detection limit of 0.05 nM [23]. Thakur et al. the electrochemical DNA aptasensor was developed for the detection of Mycobacterium tuberculosis (M. tb) antigen MPT64 by using Poly (3,4 ethylenedioxythiophene) (PEDOT) doped with carbon nanotubes [24].

In the present study, a sensitive and selective electrochemical aptasensor using anti-BPA aptamer as the recognition probe, and MWCNT/Fe_3O_4-SH@Au nanocomposite used as an immobilization platform were introduced for BPA assay. The anti-BPA aptamer was immobilized on a glassy carbon electrode modified with MWCNT/Fe_3O_4-SH@Au nanocomposite through the gold-thiol bond. The interaction between the aptamer and the BPA molecules was monitored by cyclic voltammetry (CV) and differential pulse voltammetry (DPV) in the electrochemical probe. Due to the specific affinity between BPA and anti-BPA aptamer, the conformation of aptamer showed a change after BPA binding, triggering a decrease in the electron transfer of $Fe(CN)_6^{3-/4-}$ on the electrode surface. The observed decline was detectable as a function of the presence of BPA.

Experimental

The materials, instrumentation, synthesis process of MWCNT/Fe_3O_4-SH@Au and real samples preparation are listed in the Supporting information.

Preparation of GCE/MWCNT/Fe_3O_4-SH@Au/aptamer/MCH electrode

The surface of the glassy carbon electrode was polished with alumina slurry on chamois leather until a smooth surface was obtained. Then, it was rinsed separately with ethanol and double distilled water by sound waves for 2 min, and allowed to dry at room temperature. After that, 5 μL of MWCNT/Fe_3O_4-SH@Au nanocomposite, dispersed at ethanol 1.0 mg mL^{-1}, was dropped onto GCE surface, after drying at room temperature. The electrode was named GCE/MWCNT/Fe_3O_4-SH@Au. Then, 5 μL of the aptamer solution containing 2 mM TCEP and 1 μM aptamer in 10 mM Tris-HCl buffer (pH 7.6) was casted onto the obtained electrode. For aptamer immobilization, the modified electrode was placed in a 100% moisture-saturated environment for 17 h at 4 °C. In order to eliminate the unbound aptamer, the electrode was washed with double distilled water and dried. Then 5 μL of 1 μM MCH was dropped onto the aptamer-immobilized GCE/MWCNT/Fe_3O_4-SH@Au to eliminate the non-specific adsorption of anti-BPA aptamer. After 60 min, the fabricated GCE/MWCNT/Fe_3O_4-SH@Au/aptamer/MCH biosensor was rinsed with 10 mM phosphate buffer (pH 7.6) and then, dried under N_2 stream.

For the detection of BPA, the fabricated biosensor was incubated into binding buffer (25 mM Tris HCl, pH 8.0 with 100 mM NaCl, 10 mM $MgCl_2$ and 25 mM KCl) containing 2 nM of BPA for 40 min at room temperature. Then, electrochemical measurements were performed in a probe solution containing 5.0 mM $K_3Fe(CN)_6/K_4Fe(CN)_6$ (1/1) and 0.1 M KCl. The peak current change (Δi_p) is defined by (i_0-i), where i is the anodic peak current of the aptasensor after BPA treatment while i_0 is the initial anodic peak current without BPA. The preparation procedure of MWCNT/Fe_3O_4-SH@Au/aptamer/MCH/BPA electrode is presented in Scheme 1.

Results and discussion

Characterization of MWCNT/Fe_3O_4-SH@Au nanocomposite

FT-IR was applied to confirm the immobilization of the AuNPs on the NPs, and that of Fe_3O_4-SH@Au nanocomposite on the amino-modified MWCNTs. The relevant FT-IR spectra for the preparation steps of the final nanocomposite are shown in Fig. 1. The FT-IR spectrum of Fe_3O_4NPs exhibits characteristic bands in 637, 3408 and 1625 cm^{-1} which are attributed to Fe-O and O-H stretching vibration, and to H-O-H bending vibration to in Fe_3O_4NPs, respectively. The FT-IR spectrum of the Fe_3O_4-SH@Au nanocomposite, with an absorption peak around 1432 cm^{-1}, related to aliphatic bending vibrations of CH_2 groups, also, a peak at 2800 cm^{-1} corresponding to the mercaptans stretching (-SH) in mercaptopropyl groups, were indicatior of the functionalization of magnetic nanoparticles. The presence of peaks at 3447 and 1741 cm^{-1} are related to the stretching vibrations of ν(OH) and ν(C=O) of the carboxyl groups (COOH) in the MWCNTs-NH_2. Symmetric and asymmetric methylene stretching bands at 2868 and 2923 cm^{-1}, respectively, are observed in the MWCNTs-NH_2. It is assumed that defective sites on the sidewall of MWCNTs contain these groups. Stretching vibrations of the amine group (-NH_2) overlapping with the stretching vibration of ν(-OH) in the MWCNTs-NH_2. In the FT-IR of MWCNT/Fe_3O_4-SH@Au nanocomposite, it can be seen that the absorption band around 3408 cm^{-1} decreased, indicating that the functionalized Fe_3O_4 nanoparticles modified MWCNTs-NH_2. These absorption bands show that the synthesis of MWCNT/Fe_3O_4-SH@Au nanocomposite was successful.

The surface morphology and structure of MWCNT/Fe_3O_4-SH@Au nanocomposite were investigated by FESEM and TEM. As can be seen in the FESEM image of MWCNT/Fe_3O_4-SH@Au nanocomposite in Fig. 2a, the Fe_3O_4NPs were dispersed on the MWCNTs, with a size distribution of 30–60 nm (see inset image of Fig. 2a). Moreover, the distribution of gold nanoparticles was also observable in nanocomposites. TEM

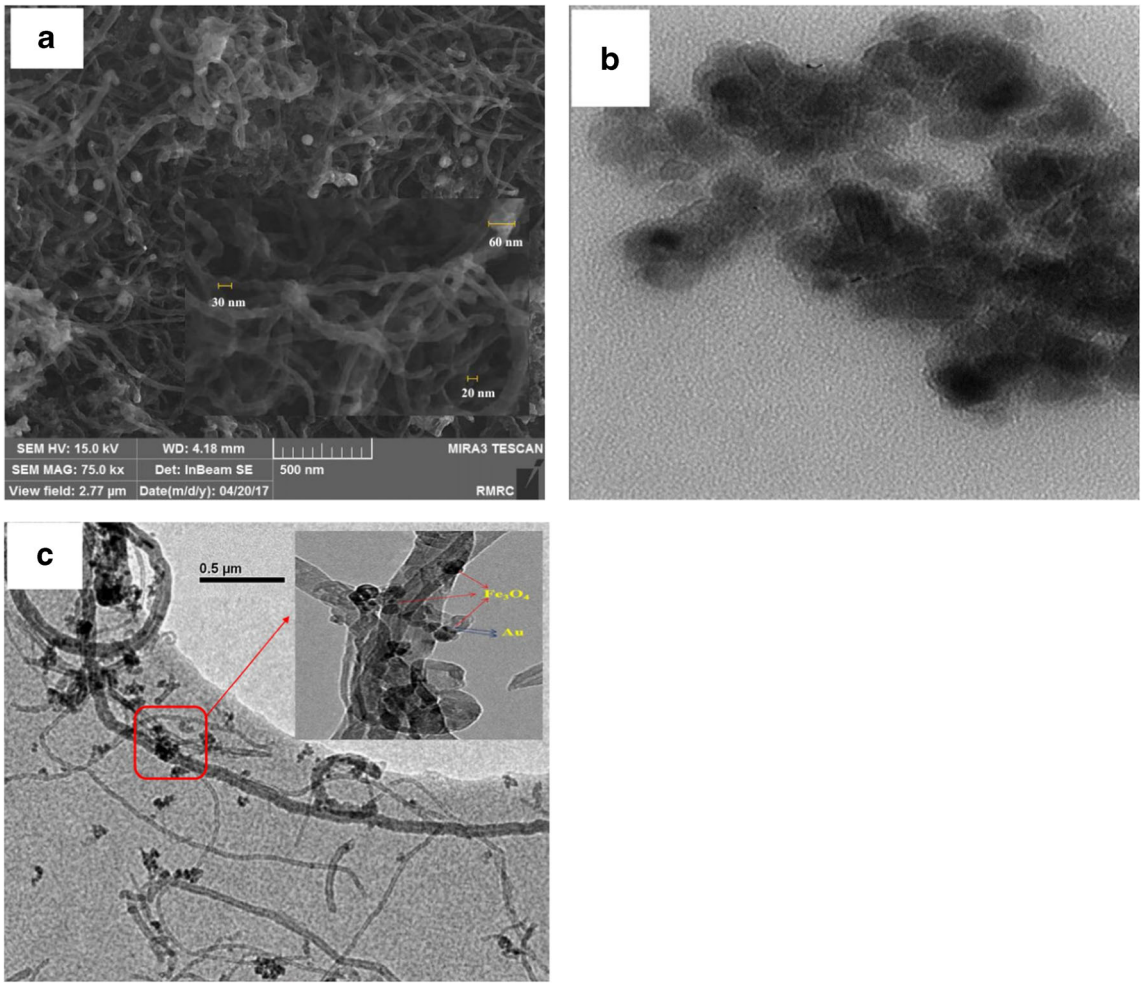

Fig. 2 **a** The FESEM image of MWCNT/Fe_3O_4-SH@Au nanocomposite. Inset: The FESEM image of MWCNT/Fe_3O_4-SH@Au with a detailed observation (**b**) TEM image of Fe_3O_4-SH@Au nanoparticle and (**c**) TEM image of MWCNT/Fe_3O_4-SH@Au nanocomposite. Inset: TEM image of MWCNT/Fe_3O_4-SH@Au nanocomposite with a detailed observation

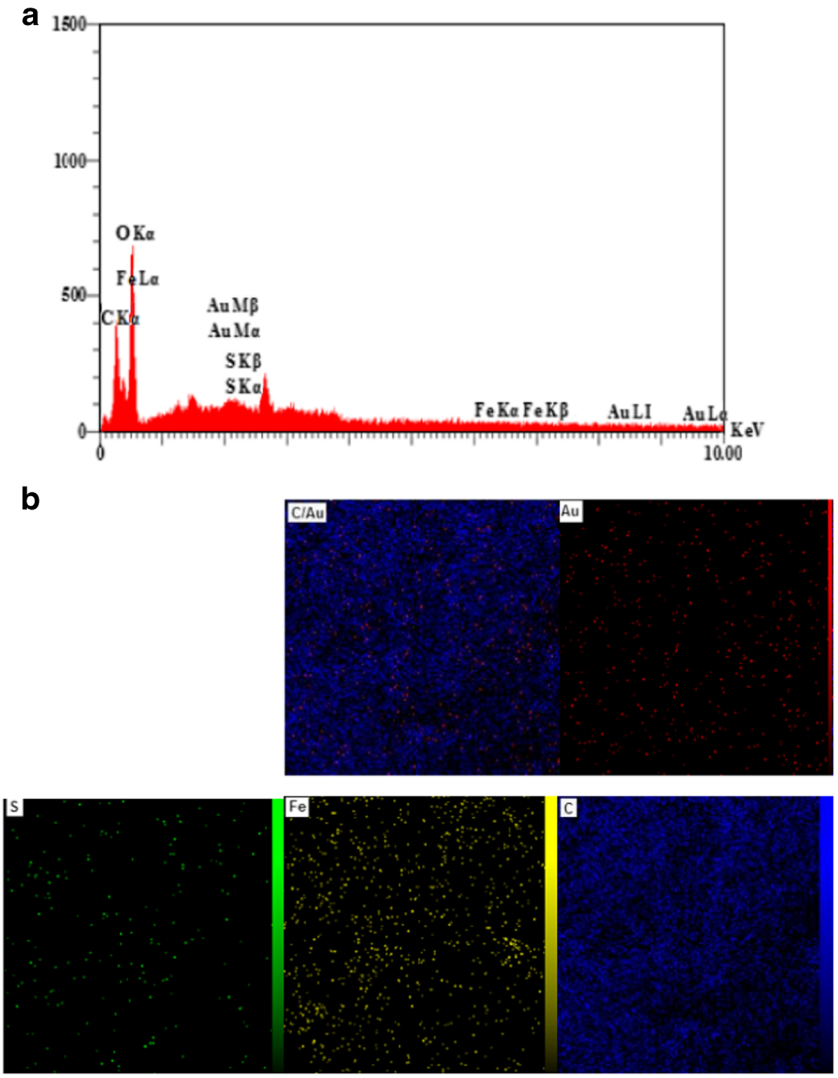

Fig. 3 **a** EDX pattern of MWCNT/Fe_3O_4-SH@Au nanocomposite. (**b**) Elemental mapping of MWCNT/Fe_3O_4-SH@Au nanocomposite

image of Fe_3O_4-SH@Au nanocomposite (Fig. 2b) reveals that Au seeds decorated on the magnetic Fe_3O_4 nanoparticles core and were immobilized on the surface of the MWCNTs (Fig. 2c). On the other hand, in TEM image of MWCNT/Fe_3O_4-SH@Au the porous network structure of MWCNTs provided a proper surface, which facilitated effective access between Fe_3O_4-SH@Au and aptamer. According to EDX patterns of MWCNT/Fe_3O_4-SH@Au nanocomposite (see Fig. 3a), the MWCNTs uniformly covered with Fe_3O_4 and Au nanoparticles. The elemental mapping analysis for the Fe_3O_4-SH@Au deposited on the MWCNTs is presented in Fig. 3b. The results confirmed that Fe_3O_4-SH and Au nanoparticles were present on the MWCNTs in the structure of nanocomposite.

The magnetic property of nanocomposite can be examined as a method to confirm the formation of MWCNT/Fe_3O_4-SH@Au nanocomposite, due to the presence of magnetic nanoparticles in prepared nanocomposite. The magnetic property of nanocomposite was characterized by VSM. The curve in Fig. 4 (curve c) shows the magnetization of the MWCNT/Fe_3O_4-SH@Au nanocomposite. The saturation magnetization of the naked

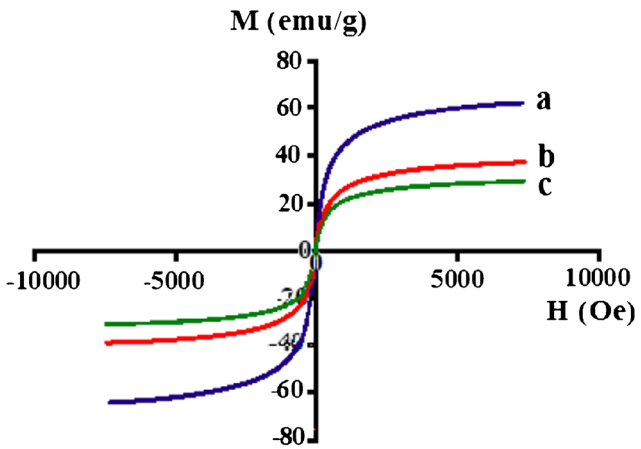

Fig. 4 Dependence of the applied magnetic field on the saturation magnetization of Fe_3O_4-SH, Fe_3O_4-SH@Au and MWCNT/Fe_3O_4-SH@Au nanocomposite

Fe_3O_4NPs was 60 emu/g (Fig. 4, curve a). As shown in Fig. 4 (curves b and c), the saturation magnetization of the Fe_3O_4-SH@Au and MWCNT/Fe_3O_4-SH@Au nanocomposite were 35 and 30 emus/g which were lower than that of the naked Fe_3O_4NPs. The decrease of saturation magnetization can be accounted for by the existence of diamagnetic AuNPs and MWCNTs in the MWCNT/Fe_3O_4-SH@Au nanocomposite. The prepared nanocomposite is super paramagnetic because no remainance and coercivity is observed at magnetization curve.

Electrochemical properties of nanocomposite were performed in order to investigat the existence of AuNPs in nanocomposite. The results listed in Supporting information.

Sensing mechanisms of the aptasensor

The designation and fabrication strategies of GCE/MWCNT/Fe_3O_4 SH@Au/aptamer/MCH for the sensing of BPA molecules are schematically depicted in Scheme 1. As shown in Fig. 5, the synergistic contribution of AuNPs, Fe_3O_4NPs and MWCNTs in MWCNT/Fe_3O_4-SH@Au nanocomposite increased the peak current. In addition, this nanocomposite provided a suitable substrate for the interaction of the -SH group at the end of anti-BPA aptamer with AuNPs through self-assembly technique. When the aptamer molecules containing 63 nucleotides were immobilized on the surface of GCE/MWCNT/Fe_3O_4-SH@Au, long tunnels were formed for the flow of electrons between bulk solution and the surface of the electrode by ($[Fe(CN)_6]^{3-/4-}$) redox system. In the absence of BPA, the conformation of the anti-BPA aptamer remained in a free configuration state, with the aptamer acting as an open-gate for the transfer of the electrons on the surface of the electrode. However, after the incubation of the BPA molecules on the fabricated electrode, an anti-BPA/BPA complex was formed, thus changing the conformation of aptamer. The G-quadruplex structure of anti-BPA/BPA complex closed the gate of the long tunnels, hindering the electron transfer on the surface of the electrode (Scheme 1). Moreover, the binding of BPA to aptamer made negative charges to appear in the back bone of the aptamer, repelling the $[Fe(CN)_6]^{3-/4-}$ anions and thus resulting in a significant decrease in the electron flux on the surface of the electrode [22].

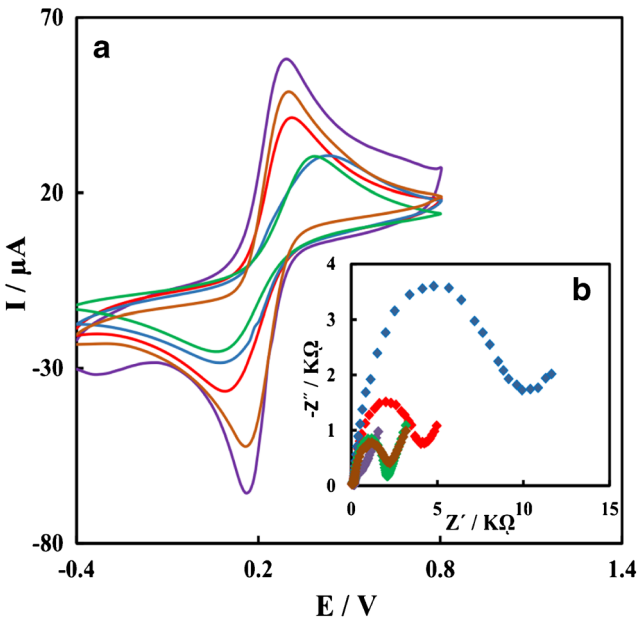

Fig. 5 **a** Cyclic voltammograms and (**b**) Nyquist plots of GCE (green line), GCE/MWCNT/Fe_3O_4-SH@Au (purple line), GCE/MWCNT/Fe_3O_4-SH@Au/aptamer (brown line), GCE/MWCNT/Fe_3O_4-SH@Au/aptamer/MCH (red line) and GCE/MWCNT/Fe_3O_4-SH@Au/aptamer/MCH/BPA (blue line) in 5 mM $Fe(CN)_6^{3-/4-}$ (1:1) solution containing 0.1 M KCl at Scan rate 0.1 V s^{-1}

Optimization the performance of aptasensor

The influence of effective parameters on detection of BPA were studied and results listed in Supporting information.

Electrochemical characterization of the aptasensor

Both cyclic voltammetry and electrochemical impedance spectroscopy (EIS) are considered powerful and valuable techniques to investigate the modification process and the electrochemical properties of an electrode. In the present study, CV and EIS measurements of the bare and modified glassy carbon electrodes were made in 5.0 mM $Fe(CN)_6^{3-}$/$Fe(CN)_6^{4-}$solution containing 0.1 M KCl. The results related to CV and EIS measurements are presented in Fig. 5, As shown in Fig. 5a, at the bare GC electrode (green line), the redox-label $Fe(CN)_6^{3-/4-}$experienced a reversible CV with a peak-to-peak separation ΔE_p of 422 mV. After GCE was casted with MWCNT/Fe_3O_4-SH@Au nanocomposite, the peak current had a dramatic increase with a ΔE_p of 140 mV. Compared to the current with bare electrode, the peak current showed an increase twice as high. However, the peak-to-peak separation potential had a significant decrease (purple line), accounted for by the synergistic effect of nanoparticles employed in the fabrication of nanocomposite, which can significantly enhance the electron transfer kinetics on the surface of electrode. When the surface of the GCE/MWCNT/Fe_3O_4-SH@Au was coated with anti-BPA aptamer, there was observed a decrease in the peak current of the $[Fe(CN)_6]^{3-/4-}$, and an increase in the peak separation (ΔE_p) compared to the GCE/MWCNT/Fe_3O_4-SH@Au electrode (Fig. 5a, brown line) indicating that the aptamer restricted the effective area and active sites necessary for electron transfer. At the next step, when the electrode was incubated with 1 mM MCH, a decreased redox peak current (Fig. 5a, red line) was obtained. Because the surface of electrode is covered with MCH and the electron transfer is carried out only via aptamer. Fig. 5a, blue line, shows the voltammogram of the GCE/MWCNT/Fe_3O_4-SH@Au/aptamer electrode incubated in 2.0 nM of BPA

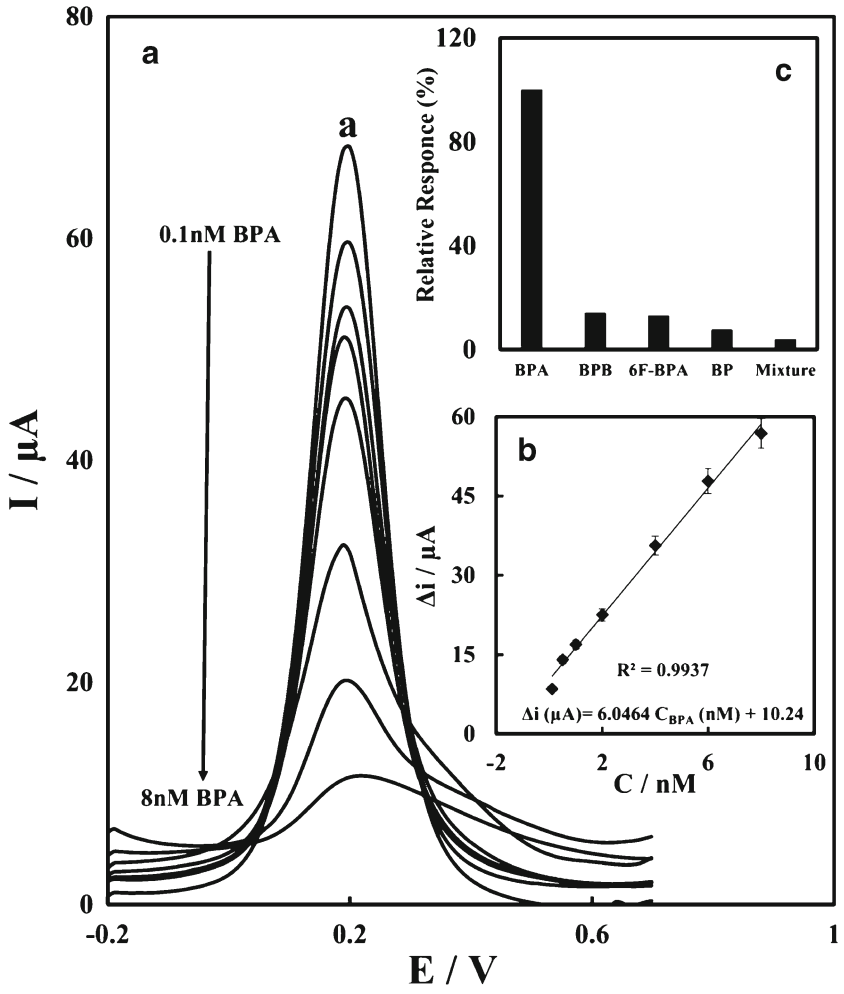

Fig. 6 **a** DPVs obtained at the GCE/MWCNT/Fe_3O_4-SH@Au/ aptamer/MCH electrode before (**a**) and after incubation in different concentration of BPA. Concentration of 0.1–8.0 nM, correspond to concentration of 0.1 (b), 0.5 (c), 1.0 (d), 2.0 (e), 4.0 (f), 6.0 (g) and 8.0 (h) nM of BPA solutions. (**b**) linear dependence of the peak current change with BPA concentration. (**c**) Selectivity confirmation studies of the proposed aptasensor for determination of BPA

Table 1 The results obtained for BPA detection in real sample ($n = 5$) using GCE/MWCNT/Fe_3O_4-SH@Au/ aptamer/MCH electrode

Sample	Added (nM)	Found (nM)	R.S.D	Recovery (%)
Mineral water	0	-	-	-
	2	2.29 ± 0.11	5.0	120.5
	8	8.37 ± 0.07	0.8	104.6
Milk	0	-	-	-
	2	2.32 ± 0.06	2.8	116.2
	8	8.25±0.01	0.2	103.0
Orange juice	0	-	-	-
	2	1.95 ± 0.10	5.0	97.5
	8	8.10±0.02	0.2	101.1

Mineral water sample (Extra, Govaranoush Co., Khorasan, Iran)

Milk sample (Pegah, Iran Dairy Industries Co., Guilan, Iran)

Orange juice sample (Sun Star, Zarin Jam Marina Co., Tehran, Iran)

solution. As can be seen, the peak current showed a decrease while the peak-to-peak separation potential had an increase. This finding can be accounted for by the fact that the formation of anti-BPA aptamer/BPA complexe blocked the diffusion of $Fe(CN)_6^{3-}/Fe(CN)_6^{4-}$ towards the electrode surface.

For a deeper evaluation of the steps taken for the modification of the electrode, the electrodes were also characterized by EIS. In Niquist plot of EIS results, the semicircle part observed at higher frequencies shows the limited process of the charge transfer while the increase of the semicircle diameter is an indication of the increase due to interfacial charge-transfer resistance (R_{ct}). As can be seen in Fig. 5b, the resistance to charge transfer in a glassy carbon electrode modified with MWCNT/Fe_3O_4-SH@Au nanocomposite was significantly reduced compared to that of the bare electrode. The bare electrode possessed a charge transfer resistance (R_{ct}) of about 2030 Ω (green line) while the glassy carbon electrode modified with nanocomposite showed a very small semicircle domain ($R_{ct} = 133.6$ Ω, purple line), proving a fast charge transfer process on the electrode surface. After the immobilization of aptamer on the modified electrode surface, the R_{ct}

value increased to 2130 Ω (brown line), indicating a strong interaction between the thiolated aptamer and AuNPs. When the MCH incubated on the surface electrode, the R_{ct} value increased to 4048 Ω (red line), it shows that the electron transfers of redox probe blocked on the surface of electrode. Consequently, when the aptasensor was incubated with 2.0 nM BPA for 30 min, an increase in R_{ct} was observed (R_{ct} = 10,000 Ω, bule line), proving successful formation of an anti-BPA aptamer/BPA complex and a surface blocking for charge transfer of redox system. These results are in line with that observed in CV investigation.

Analytical performance of the electrochemical aptasensor

DPV was utilized to quantitatively detect BPA after the optimization of various parameters affecting the response peak current. Fig. 6a shows the DPVs of GCE/MWCNTs/Fe_3O_4-SH@Au/aptamer/MCH incubated at different concentrations of BPA in 5 mM $Fe(CN)_6^{3-/4-}$ containing 0.1 M KCl. As shown in Fig. 6a, the peak current response of $Fe(CN)_6^{3-/4-}$ probe was negatively correlated with BPA concentration in that it decreased as the BPA concentration increased. However, the peak current change (Δi) increases. Fig. 6b shows a linear relationship between BPA concentration and the magnitude of Δi_{DPV}, for BPA detections between 0.1–8 nM with a detection limit of 0.03 nM BPA (S/N = 3). The reproducibility of the sensor was confirmed through repeating the measurements for five similarly prepared modified electrodes at the same concentration of BPA. The standard derivation (RSD) was 4.4%, showing a good reproducibility of the fabricated aptasensor in the determination of BPA. The long-term stability of GCE/MWCNT/Fe_3O_4-SH@Au/aptamer/MCH was also studied. To this end, the GCE/MWCNT/Fe_3O_4-SH@Au/aptamer/MCH was kept at 4 °C in a refrigerator for 7 days, and then was analyzed at the same BPA concentration level. The current change (Δi) was 4.7% (lower than 5%), which confirms that the aptasensor enjoyed a good stability. The proposed aptasensor was compared with a variety of fabricated aptasensors and methods to determine the BPA (Table S1 at Supporting information). In comparison with the other methods for the determination of BPA, the BPA detection method presented in this study showed relatively low detection limits and wide linear ranges.

The excellent selectivity is an important characteristic of the GCE/MWCNT/Fe_3O_4-SH@Au/aptamer/MCH aptasensor. The selectivity of the BPA aptasensor was tested by using three types of BPA analogs (BPB, BP and 6F-BFA) as the interferons. The Δi value for pure BPA was set as 100%, the Δi values in the solutions containing three interferons had fluctuations within 0.4 and 13.8% showing a good selectivity of the aptasensor (Fig. 6c). Even when all three other interferons were mixed with BPA, the current change was lower than 3.7%.

Real sample analysis

The modified GCE was used to detect BPA in a samples such as mineral water, milk, and juice samples in order to evaluate its practical performance. The Results are summarized in Table 1. As shown in Table 1, the values of recovery are between 97.5 and 120.5% with RSDs of 0.2–5.0%, showing that the aptasensor is efficient in determining the BPA.

Conclusions

In the present study, a novel apasensor, based on MWCNTs, AuNPs and Fe_3O_4NPs, was fabricated for an effective sensing of BPA. The results of the analyses done showed that the MWCNT/Fe_3O_4-SH@Au nanocomposite provided a suitable substrate for aptamer interaction, Moreover, the results showed that it facilitated the electron transfer rate at the electrode surface. Due to the special affinity between anti-BPA aptamer and BPA molecules, the BPA aptasensor enjoyed excellent sensitivity and selectivity for the determination of BPA in real samples. Moreover, the BPA aptasensor proposed in the present study exhibited a linearity index between 0.1 and 8 nM, and a low detection limit of 0.03 nM for BPA. These results obtained are accounted for by the synergistic effect of combining MWCNTs, Fe_3O_4NPs with AuNPs, aptamer, and MCH. As the results of the use of the proposed aptasensor on real samples showed, it has valuable potential applications in food industries where a fast and reliable detection of BPA is of paramount importance for the health of the public.

Acknowledgements We would like to thank the post-graduate office of Guilan University and Hakim Sabzevari University for the support of this work.

Compliance with ethical standards The author(s) declare that they have no competing interests.

References

1. Mirzajani H, Cheng C, Wu J, Chen J, Eda S, Aghdam EN, Ghavifekr HB (2017) A highly sensitive and specific capacitive aptasensor for rapid and label-free trace analysis of bisphenol a in canned food. Biosens Bioelectron 89:1059–1067
2. An analysis of European plastics production, demand and waste data. http://www.plasticseurope.org/Document/plastics-the-facts/, 2014 (accessed 15.01.22)
3. Hadavifar M, Bahramifar N, Younesi H, Li Q (2014) Adsorption of mercury ions from synthetic and real wastewater aqueous solution by functionalized multi-walled carbon nanotube with both amino and thiolated groups. Biochem Eng J 237:217
4. Temel NK, Gürkan R (2017) A micellar sensitized kinetic method for quantification of low levels of bisphenol a in foodstuffs by spectrophotometry. Anal Methods 9:1190–1200

5. Filippou O, Deliyanni EA, Samanidou VF (2016) Fabrication and evaluation of magnetic activated carbon as adsorbent for ultrasonic assisted magnetic solid phase dispersive extraction of bisphenol a form milk prior to high performance liquid chromatographic analysis with ultraviolet detection. J Chromatogr A 1479:20
6. Zimmers SM, Browne EP, O'Keefe PW, Anderton DL, Kramer L, Reckhow DA, Arcaro KF (2014) Determination of free bisphenol a concentrations in breast milk of U.S. women using a sensitive LC/MS/MS method. Chemosphere 104:237
7. Pastor-Belda M, Bastida D, Campillo N, Pérez-Cárceles MD, Motas M, Vinas P (2016) A study of the influence on diabetes of free and conjugated bisphenol a concentration in urine: development of a simple microextraction procedure using gas chromatography–mass spectrometry. J Pharm Biomed Anal 129:458–465
8. Zhang X, Zhu D, Huang C, Sun Y, Lee Y (2015) Sensitive detection of bisphenol a in complex samples by in-column molecularly imprinted solid-phase extraction coupled with capillary electrophoresis. Microchem J 121:1–5
9. Xue F, Wu J, Chu H, Mei Z, Ye Y, Liu J, Zhang R, Peng C, Chen W (2013) Electrochemical aptasensor for the determination of bisphenol a in drinking water. Microchim Acta 180:109–115
10. Li O, Zhai X, Liu X, Wang L, Liu H, Wang H (2016) Electrochemical determination of bisphenol a at ordered mesoporous carbon modified nano-carbon ionic liquid paste electrode. Talanta 148:362–369
11. Alsaafin A, McKeague M (2017) Functional nucleic acids as in vivo metabolite and ion biosensors. Biosens Bioelectron 94:94–106
12. Rapini R, Marrazza G (2017) Electrochemical aptasensors for contaminants detection in food and environment: recent advances. Bioelectrochemistry 118:47–61
13. Zhu Y, Zhou C, Yan X, Yan Y, Wang Q (2015) Aptamer-functionalized nanoporous gold film for high-performance direct electrochemical detection of bisphenol a in human serum. Anal Chim Acta 883:81–89
14. Liu Y, Zhang X, Yang J, Xiong E, Zhang X, Chen J (2016) Sensitive detection of bisphenol a based on a ratiometric electrochemical aptasensor. Can J Chem 94:509–514
15. Derikvand Z, Abbasi AR, Roushani M, Derikvand Z, Azadbakht Z (2016) Design of ultra- sensitive bisphenol A-aptamer based on Pt nanoparticles loading to polyethyleneimine functionalized carbon nanotubes. Anal Biochem 512:47–57
16. Cui H, Wu J, Eda S, Chen J, Chen W, Zheng L (2015) Rapid capacitive detection of femtomolar levels of bisphenol a using an aptamer-modified disposable microelectrode array. Microchim Acta 182:2361–2367
17. Ebrahimpour E, Amiri A, Baghayeri M, Rouhi M, Lakouraj MM (2017) Poly (indole-co-thiophene)@Fe_3O_4 as novel adsorbents for the extraction of aniline derivatives from water samples. Microchem J 131:174–181
18. Rouhi M, Lakouraj MM, Baghayeri M, Hasantabar V (2017) Novel conductive magnetic nanocomposite based on poly (indole-co-thiophene) as a hemoglobin diagnostic biosensor: synthesis, characterization and physical properties. Int J Polymer Mater 66:12–19
19. Baghayeri M, Zare EN, Lakouraj MM (2014) A simple hydrogen peroxide biosensor based on a novel electro-magnetic poly(p-phenylenediamine)@Fe_3O_4 nanocomposite. Biosens Bioelectron 55:259–265
20. Wang J (2012) Electrochemical biosensing based on noble metal nanoparticles. Microchim Acta 177:245–270
21. Tian Y, Chen L, Zhang J, Ma Z, Song C (2012) Bifunctional au-nanorod@Fe_3O_4 nanocomposites: synthesis, characterization, and their use as bioprobes. J Nanopart Res 14:998
22. Zhou L, Wang J, Li D, Li Y (2014) An electrochemical aptasensor based on gold nanoparticles dotted graphene modified glassy carbon electrode for label-free detection of bisphenol a in milk samples. Food Chem 162:34–40
23. Deiminiat B, Rounaghi GH, Arbab-Zavar MH, Razavipanah I (2016) A novel electrochemical aptasensor based on f-MWCNTs/AuNPs nanocomposite for label-free detection of bisphenol a. Sensors Actuators B Chem 242:158
24. Thakur H, Kaur N, Sareen D, Prabhakar N (2017) Electrochemical determination of M. Tuberculosis antigen based on poly(3,4-ethylenedioxythiophene) and functionalized carbon nanotubes hybrid platform. Talanta 171:115